Solution Self-Assembly of Block Copolymers Containing a Branched Hydrophilic Block into Inverse Bicontinuous Cubic Mesophases

Tae Hyun An,[†] Yunju La,[†] Arah Cho,[†] Moon Gon Jeong,[†] Tae Joo Shin,[‡] Chiyoung Park,[*,†] and Kyoung Taek Kim[*,†,§]

[†]Department of Chemistry, Ulsan National Institute of Science and Technology (UNIST), 50 UNIST Road, Ulsan 689-798, Korea, [‡]Pohang Accelerator Laboratory, POSTECH, Pohang 790-784, Korea, and [§]KIST-UNIST-Ulsan Center for Convergence Materials, Ulsan 689-798, Korea

ABSTRACT Solution self-assembly of amphiphilic block copolymers into inverse bicontinuous cubic mesophases is an emerging strategy for directly creating highly ordered triply periodic porous polymer nanostructures with large pore networks and desired surface functionalities. Although there have been recent reports on the formation of highly ordered triply periodic minimal surfaces of self-assembled block copolymer bilayers, the structural requirements for block copolymers in order to facilitate the preferential formation of such inverse mesophases in solution have not been fully investigated. In this study, we synthesized a series of model block copolymers, namely, branched poly(ethylene glycol)-*block*-polystyrene (bPEG-PS), to investigate the effect of the architecture of the block copolymers on their solution self-assembly into inverse mesophases consisting of the block copolymer bilayer. On the basis of the results, we suggest that the branched architecture of the hydrophilic block is a crucial structural requirement for the preferential self-assembly of the resulting block copolymers into inverse bicontinuous cubic phases. The internal crystalline lattice of the inverse bicontinuous cubic structure can be controlled *via* coassembly of branched and linear block copolymers. The results presented here provide design criteria for amphiphilic block copolymers to allow the formation of inverse bicontinuous cubic mesophases in solution. This may contribute to the direct synthesis of well-defined porous polymers with desired crystalline order in the porous networks and surface functionalities.

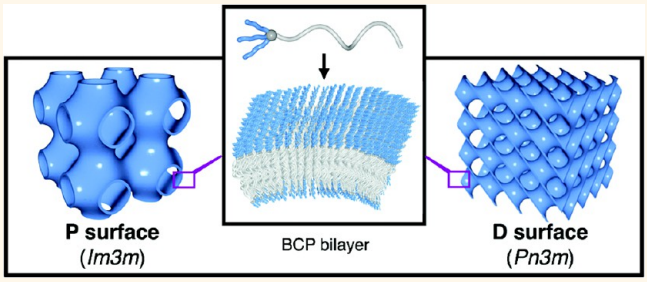

KEYWORDS: block copolymers · self-assembly · mesoporous polymers · minimal surfaces · polymer cubosomes

Solution self-assembly of amphiphilic block copolymers (BCPs) has been extensively used for the creation of nanostructures with desired size, shape, and physicochemical functions.[1−6] By taking advantage of the relationship between the chemical structure and self-assembly behavior of amphiphiles,[7−10] the structural parameters of the amphiphilic BCPs such as the molecular weights of incompatible polymer blocks and their relative ratio have been manipulated to direct the self-assembly of BCPs. This has facilitated the "bottom-up" creation of nanoscaled objects with desired morphology, spanning from simple spherical micelles to cylindrical micelles and polymer vesicles.[11−24] In this context, a relatively unexplored field in the solution self-assembly of BCPs is the formation of inverse phases.[25−28] When the critical packing factor (P) of a lipid (defined as $P = V/a_0 l_c$, where V is the volume of the hydrophobe, a_0 is the molecular area per amphiphile, and l_c is the critical length of the hydrophobe) exceeds unity, the flat lipid bilayer develops a negative curvature.[29−31] To minimize the surface area, the curved bilayer evolves into triply periodic minimal surfaces (TPMSs) possessing net zero curvature throughout the surface.[32−37] The resulting inverse bicontinuous cubic mesophases of lipid bilayers and their emulsified nanoparticles (cubosomes)[38−41] internalize nanoporous networks arranged in the cubic crystalline order. These structures have attracted recent attention as platforms for the crystallization

* Address correspondence to cpark@unist.ac.kr, ktkim@unist.ac.kr.

Received for review December 23, 2014 and accepted March 3, 2015.

Published online March 03, 2015
10.1021/nn507338s

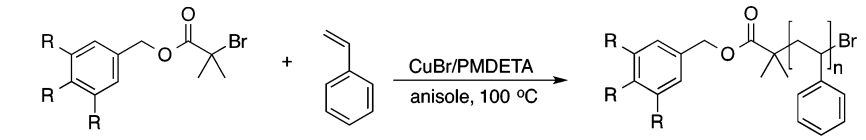

550_3-Br R = $CH_3(OCH_2CH_2)_{12}O$
750_3-Br R = $CH_3(OCH_2CH_2)_{17}O$

550_3-PS_n R = $CH_3(OCH_2CH_2)_{12}O$
750_3-PS_n R = $CH_3(OCH_2CH_2)_{17}O$

Scheme 1. Synthesis of bPEG-PS.

of membrane proteins,[42,43] as additives of food products,[44−47] and as vehicles for the sustained release of pharmaceutical cargo molecules.[48−61] The polymeric analogues of the inverse bicontinuous cubic structures of lipids could serve as unique platforms for highly defined porous polymers potentially useful for applications such as separation and templating.

In solution, BCPs have been shown to form inverse mesophases similar to those exhibited by self-assembly of lipids.[62−74] Eisenberg and co-workers reported the formation of inverse hexagonal phases within the self-assembled nanoparticles (hexasomes) of poly(acrylic acid)-*b*-polystyrene (PAA-*b*-PS) in solution.[63−65] Sommerdijk and co-workers demonstrated the formation of nanoparticles with internal bicontinuous porous networks from the self-assembly of the block copolymers consisting of a linear poly(ethylene glycol) and brushed hydrophobic blocks in water.[66−72] Of particular interest is the formation of inverse bicontinuous cubic crystalline structures of BCP bilayers in solution because this direct self-assembly allows the resulting materials to possess highly organized internal mesoporous networks reticulated in 3-D crystalline lattices.

We previously reported that dendritic-linear BCPs with a dendritic hydrophilic block preferentially self-assembled into colloidal particles consisting of inverse bicontinuous cubic phases of BCP bilayers (polymer cubosomes).[73,74] The internal structures of the polymer cubosomes closely resembled the corresponding lipid structures, which exhibited the enlarged periodicity and pore diameter arising from the high molecular weight polymeric building blocks. The minimal surfaces of the BCP bilayers were observed to have Schwartz P and D and Schoen G structures[75] in the polymer cubosomes, depending on the architecture of the dendritic hydrophilic block. Recently, Peinemann and co-workers also reported that a linear BCP, poly(acrylic acid)-polystyrene (PAA-PS), with a short PAA block, self-assembled into polymer cubosomes having Schwartz P internal structure in a methanol/toluene mixture.[76] Although such reports exist along with previous observations of colloidal particles of inverse mesophases of BCPs,[77−82] the underlying mechanism of the self-assembly leading to the formation of inverse bicontinuous cubic mesophases of BCPs has not been fully understood. Consequently, the structural parameters of the BCPs that are required for the formation of inverse bicontinuous phases have not been clearly explained.

TABLE 1. Characterization of bPEG-PSs and a Linear Analogue

sample	M_n (g mol^{-1})[a]	$Đ$[a]	DP_n (PS)[b]	f_{PEG} (%)[c]	phase[d]
550_3-PS_{183}	20 520	1.07	183	9.0	v
550_3-PS_{212}	23 470	1.08	212	7.8	c
550_3-PS_{231}	24 580	1.08	231	7.1	lc
PEG_{45}-PS_{228}	24 750	1.12	228	8.7	v
750_3-PS_{363}	39 480	1.04	363	6.2	v
750_3-PS_{390}	42 500	1.09	390	5.7	c
750_3-PS_{413}	44 500	1.16	413	5.4	lc
750_3-$(PS_{57})_2$	16 090	1.04	114	19.7	c

[a] The number-average molecular weight and molecular weight distribution determined by GPC (THF, 35 °C, 1 mL min^{-1} flow rate) using PS standards. [b] The number-average degree of polymerization of the PS block determined by ^{1}H NMR integration. [c] The molecular weight ratio of the PEG domain to that of the PS block (M_n(PEG) = 1650 g mol^{-1} for 550_3-PS_n, 2000 g mol^{-1} for PEG_{45}-PS_n, and 2250 g mol^{-1} for 750_3-PS_n). [d] Observed morphology of self-assembled structures of the suspension solution prepared from a dioxane solution of the BCP (0.5 wt %). v: vesicle, c: cubosomes, lc: large cubosomes.

Here we report the formation of polymer cubosomes consisting of inverse bicontinuous cubic structures of the self-assembled bilayer of the BCPs composed of a branched hydrophilic block and a linear hydrophobic block. We designed and synthesized these BCPs as a model system to investigate the effect of the architecture of the BCPs on their preferential self-assembly into inverse bicontinuous cubic mesophases. Our results suggest that the presence of branched architecture in the hydrophilic block is a crucial structural requirement for self-assembly of BCPs to inverse mesophases. We also show that the crystalline structure of the inverse cubic phases of BCPs could be controlled to have the desired symmetry by simple coassembly of two BCPs. Our results reported here may provide a design rule of BCPs for the synthesis of highly ordered triply periodic mesoporous polymers.

RESULTS AND DISCUSSION

BCPs with a Branched Hydrophilic Block and Their Self-Assembly in Solution. We synthesized BCPs consisting of a hydrophilic block having three poly(ethylene glycol) (PEG) branches and a linear polystyrene hydrophobic block (bPEG-PS) (Scheme 1). Two series of bPEG-PSs were prepared by the atom-transfer radical polymerization (ATRP) of styrene using macroinitiators 550_3-Br (three PEG chains with M_n = 550 g mol^{-1}) and 750_3-Br (three PEGs with M_n = 750 g mol^{-1}). The length of the

PS block was adjusted so that the resulting BCPs have a desired block ratio (defined by f_{PEG}, a ratio of the molecular weight of the PEG domain and that of the PS block).[83] The resulting bPEG-PSs, 550_3-PS_n and 750_3-PS_n (n represents the degree of polymerization of the PS block, as measured by ^{1}H NMR integration) showed a narrow molecular weight distribution, as determined by gel permeation chromatography (GPC) (Table 1).

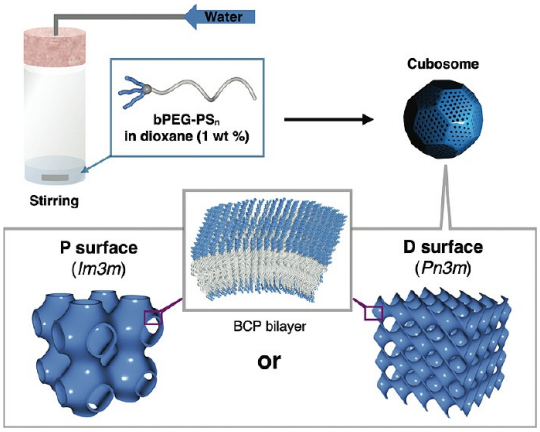

Figure 1. Self-assembly of bPEG-PS into polymer cubosomes consisting of an inverse bicontinuous cubic crystalline structure of block copolymer bilayers.

(For details of synthesis and characterization of macroinitiators and bPEG-PSs, see the Supporting Information (SI).)

The resulting BCPs were allowed to self-assemble in an aqueous solution by the cosolvent method (Figure 1). Typically, the bPEG-PSs were dissolved in 2 mL of dioxane (1 wt %). Water, a selective solvent for the PEG block, was added at a controlled rate (1 mL h^{-1}) to the dioxane solution of the BCP with stirring, until the volume fraction of water in the dispersion reached 50%. After dialysis against water for 24 h to remove the organic solvent, the resulting aqueous suspension was studied by scanning electron microscopy (SEM), transmission electron microscopy (TEM), and synchrotron small-angle X-ray scattering (SAXS).

Self-assembled structures of 550_3-PS_n in aqueous solution underwent a transition of morphology from polymer vesicles and flat lamella (Figure 2A) to polymer cubosomes of varying diameters (Figure 2B,C and Figure 3) upon increasing the molecular weight of the PS block, which resulted in a decrease in the f_{PEG} value. Further increase in the molecular weight of the PS block yielded colloidal particles having internal inverse hexagonal structures (hexasomes) (Figure S5 in the SI). The average diameter (D_{av}) of the polymer cubosomes, determined by analyzing low-magnification

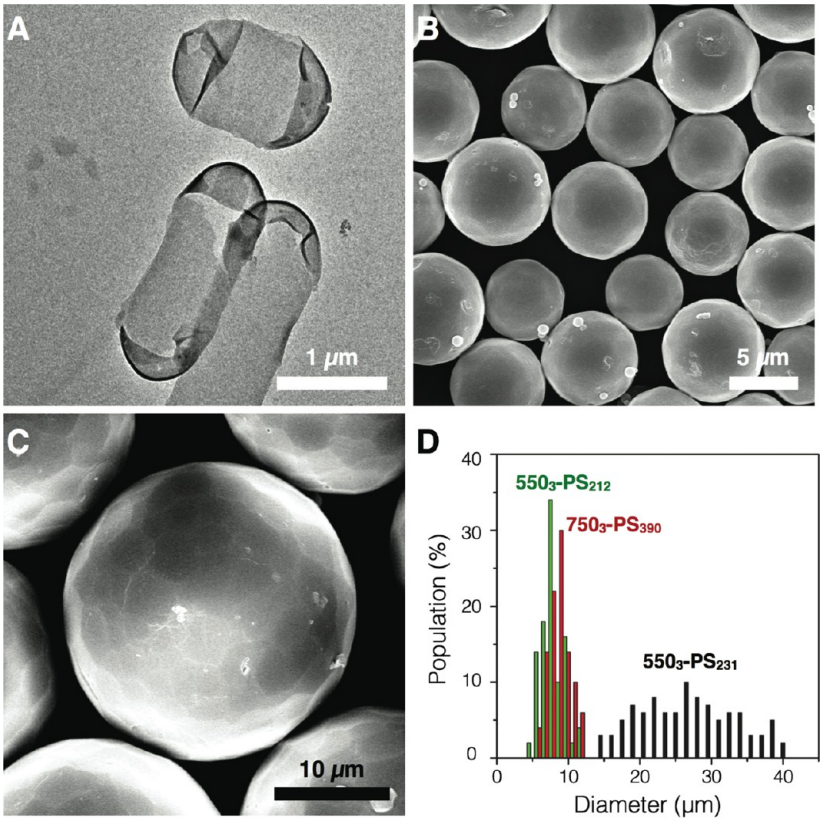

Figure 2. Phase transition of self-assembled structures of 550_3-PS_n in solution on increasing the molecular weight of the PS block. (A) Flat bilayer and polymersomes of 550_3-PS_{183}. (B) Polymer cubosomes of 550_3-PS_{212}. (C) Large polymer cubosomes of 550_3-PS_{231}. (D) Distributions of the diameter of polymer cubosomes of 550_3-PS_{212} (green bars, average diameter of 7.6 μm) and 550_3-PS_{231} (black bars, average diameter of 28.2 μm).

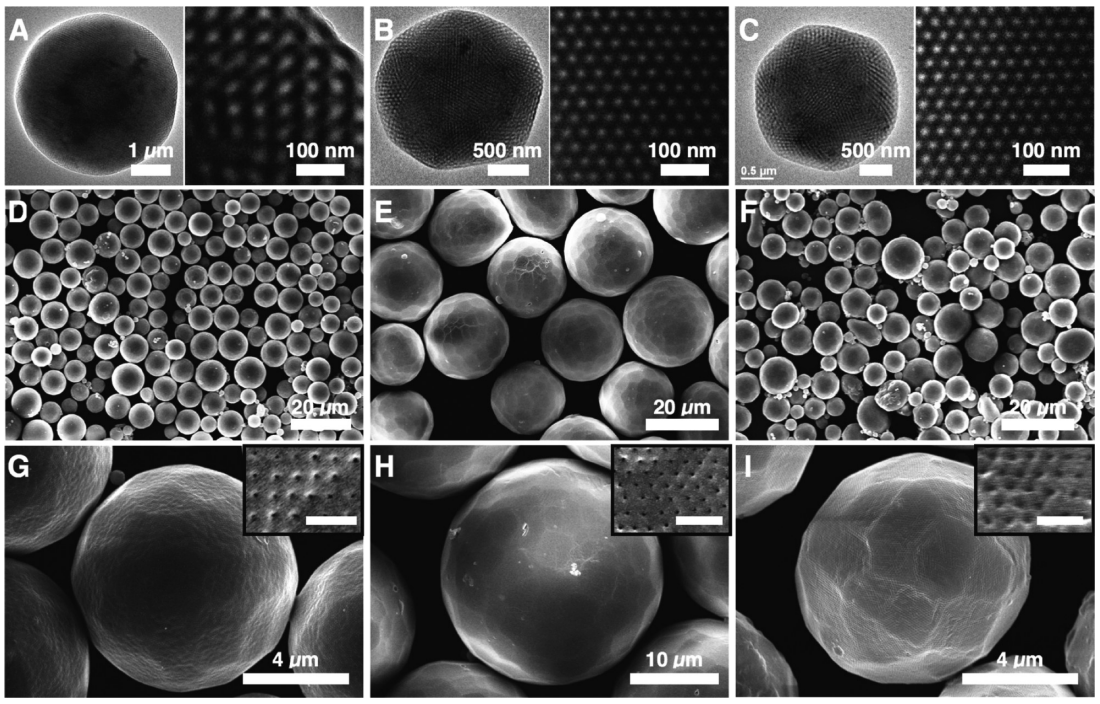

Figure 3. Electron micrographs of polymer cubosomes of bPEG-PSs. (A–C) TEM images of the internal structures of polymer cubosomes: (A) 550_3-PS_{212}, (B) 550_3-PS_{231}, and (C) 750_3-PS_{390}. (D, E) SEM images of polymer cubosomes showing size distribution: (D) 550_3-PS_{212}, (E) 550_3-PS_{231}, and (F) 750_3-PS_{390}. (G–I) High-magnification SEM images of individual polymer cubosomes. The insets show the perforated surface layer of the polymer cubosomes (scale bars are 200 nm). (G) 550_3-PS_{212}, (H) 550_3-PS_{231}, and (I) 750_3-PS_{390}.

SEM images (100 particles), was 7.6 μm for the polymer cubosomes of 550_3-PS_{212} (f_{PEG} = 7.8%) and 28.2 μm for those of 550_3-PS_{231} (f_{PEG} = 7.1%) (Figure 2D). In addition, we observed an identical transition of morphology of the self-assembled structures of 750_3-PS_n depending on the molecular weight of the PS block (Figure S6 in the SI). Interestingly, the f_{PEG} value of 750_3-PS_n corresponding to the formation of polymer cubosomes was ~5%, which was lower than those for the formation of the polymer cubosomes of 550_3-PS_n (Table 1). Considering that the lower critical solution temperatures (LCSTs) of oligo(ethylene glycol)s increase with an increase in the number of repeating units,[84,85] the requirement for long hydrophobic PS chains for the formation of inverse mesophases of 750_3-PS_n might arise from the increased hydrophilicity of the branched blocks consisting of PEG chains, which are longer than the hydrophilic block of 550_3-PS_n.

For comparison, we synthesized linear BCPs, PEG_{45}-PS_n with f_{PEG} values similar to those of bPEG-PSs forming inverse mesophases. Under identical conditions of self-assembly as the bPEG-PSs, the linear analogues self-assembled only into polymer vesicles (polymersomes), indicating that the branched–linear architecture of bPEG-PSs likely plays an important role in the preferential self-assembly of bPEG-PS into inverse mesophases in solution. It should be noted that the block ratio, which is indicated by the f_{PEG} value, was a key factor determining the self-assembly of bPEG-PSs into inverse cubic mesophases rather than into lamellar or inverse hexagonal phases. These results strongly suggested that the presence of the branched architecture in the hydrophilic block was an essential structural requirement for the self-assembly of bPEG-PSs into inverse bicontinuous cubic mesophases in solution.

Structural Analysis of Polymer Cubosomes. Next, we examined, in detail, the internal structures of the inverse bicontinuous cubic phases of the polymer cubosomes by synchrotron SAXS (Figure 4). The SAXS results of the polymer cubosomes of 550_3-PS_{212} showed *Im*3*m* symmetry (lattice constant a = 93.4 nm), suggesting that the internal inverse phase consisted of a Schwartz P surface. In contrast, the SAXS pattern of the polymer cubosomes of 550_3-PS_{231} exhibited *Pn*3*m* symmetry (a = 45.3 nm), indicating that the internal structure consisted of a Schwartz D surface. High-resolution SEM images of the fractured polymer cubosomes of 550_3-PS_{212} and 550_3-PS_{231} (Figure 4A and B) further confirmed that these internal structure assignments for the polymer cubosomes were matched to the structures assigned by the SAXS patterns. TEM images of the internal structures of the polymer cubosomes also revealed the presence of crystalline structures consisting of minimal surfaces of the BCP bilayer. On the other hand, SAXS results obtained from the polymer cubosomes of 750_3-PS_{390} and 750_3-PS_{413} showed peaks corresponding only to *Pn*3*m* symmetry (a = 64.2 nm for the polymer cubosomes of 750_3-PS_{390}), indicating that the internal inverse bicontinuous cubic structure was a Schwartz D surface (Figure 4E).

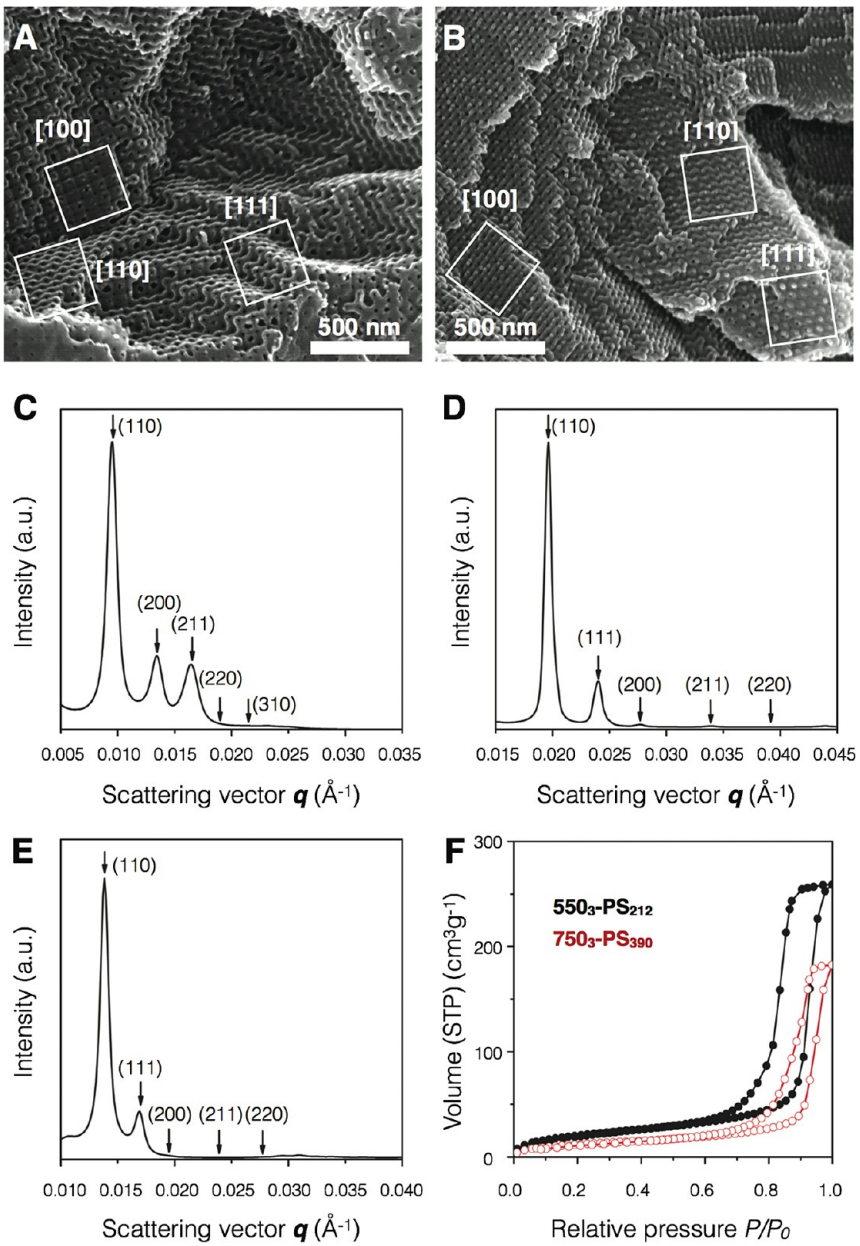

Figure 4. Structural characterization of the internal crystalline structures of polymer cubosomes. (A) SEM images of the internal P surface structure of the polymer cubosomes of 550_3-PS_{212}. The areas marked with boxes show different planes viewed in the [100], [110], and [111] directions. (B) SEM images of the internal D surface structure of the polymer cubosomes of 550_3-PS_{231}. The areas marked with boxes show different planes viewed in the [100], [110], and [111] directions. (C) SAXS results of the polymer cubosomes of 550_3-PS_{212} show *Im*3*m* symmetry (lattice constant $a = 93.4$ nm), indicating that the internal structure is a P surface. (D, E) SAXS results of the polymer cubosomes of 550_3-PS_{231} (D) and 750_3-PS_{390} (E) show *Pn*3*m* symmetry ($a = 45.3$ nm for 550_3-PS_{231} and $a = 64.2$ nm for 750_3-PS_{390}), indicating that the internal structure is a D surface. (F) N_2 adsorption−desorption isotherms at 77 K of the polymer cubosomes of 550_3-PS_{212} (black filled circles) and 750_3-PS_{390} (red empty circles).

The change in the internal crystalline structure of the polymer cubosomes of 550_3-PS_n with increasing n was attributed to an increase of the local curvature of the bilayer membrane constituting the inverse mesophases. For a hydrophilic block with a fixed molecular weight, the increase in the molecular weight of the PS block would lead to an increase in volume of the hydrophobic domain, which, in turn, may allow the self-assembled bilayer to adopt a higher curvature. This hypothesis may be justified by considering that the lipid having a larger volume of the hydrophobic chain formed an inverse cubic phase with *Pn*3*m* symmetry, rather than a structure with *Im*3*m* symmetry.[30,31]

The polymer cubosomes of bPEG-PS consisted of bilayers of BCPs with high-molecular-weight glassy PS hydrophobic blocks. Therefore, the polymer cubosomes of bPEG-PSs were structurally robust under ambient conditions, which allowed these colloidal particles to transform into mesoporous polymers upon the removal of water. Type IV isotherms with type H2

hysteresis loops were observed in the N_2 adsorption–desorption experiments carried out at 77 K, which indicated the presence of bicontinuous porous networks within the polymer cubosomes (Figure 4F). The polymer cubosomes of 550_3-PS_{212} possessed a Brunauer–Emmett–Teller (BET) surface area of 77.7 $m^2\ g^{-1}$ and a pore volume of 0.45 $cm^3\ g^{-1}$. The Barrett–Joyner–Halenda (BJH) pore size distribution analysis revealed the presence of pores with a broad size distribution and a peak diameter of 26.4 nm. The polymer cubosomes of 750_3-PS_{390} exhibited isotherms similar to those of the polymer cubosomes of 550_3-PS_{212} and had a BET surface area and pore volume of 45.5 $m^2\ g^{-1}$ and 0.31 $cm^3\ g^{-1}$, respectively. The BJH pore size distribution analysis indicated an average pore diameter of 30.3 nm for the polymer cubosomes of 750_3-PS_{390}. These results confirmed that the polymer cubosomes of bPEG-PS were mesoporous polymers with highly organized large-pore networks arranged in crystalline order.

Effect of the Architecture of the Hydrophilic Block on the Formation of Inverse Bicontinuous Cubic Structures. For the self-assembly of lipids into inverse mesophases, the critical packing factor *P* for the lipid was presumed to be greater than unity. With an increase in the value of *P* of the lipid, the self-assembled inverse mesophases in water underwent a morphological transition from the flat lamella ($P = 1$) to Schwartz P (*Im*3*m* symmetry), Schwartz D (*Pn*3*m* symmetry), Schoen G (*Ia*3*d* symmetry), inverse hexagonal (H_{II}), and inverse micelle structures.[86,87] Given that the hydrophilic head groups were identical, this morphological transition of the inverse mesophases of lipids was closely related to the increase in the volume of the hydrophobic chain of the lipid.[30,31]

In the case of bPEG-PS, the block ratio (f_{PEG}) played a decisive role in directing the self-assembly behavior of the BCP, leading to the preferential formation of inverse mesophases. However, PEG_{45}-PS_n, the linear analogues of bPEG-PSs possessing similar block ratios, self-assembled only into polymersomes under identical conditions of self-assembly. This observation strongly suggests that the branched architecture of the hydrophilic block contributes to the increase in the value of *P* of the BCP.

To study the effect of the architecture of the hydrophilic block of bPEG-PS on its self-assembly, we first measured the molecular area of the bPEG-PS from the Langmuir isotherms at the air–water interface (Figure 5A). For amphiphilic BCPs containing PEG as the hydrophilic block, the molecular area of the block copolymer was dependent on the size of the PEG chain immersed in water and virtually independent of the size of the hydrophobic block.[83,88] The area occupied by the linear BCP PEG_{45}-PS_{185} in the monolayer at the air–water interface was measured to be 1080 $Å^2$. Similarly, the molecular areas of 550_3-PS_{183} and 750_3-PS_{185} were determined to be 1340 and 1500 $Å^2$, respectively. These results suggested that the branched architecture of the

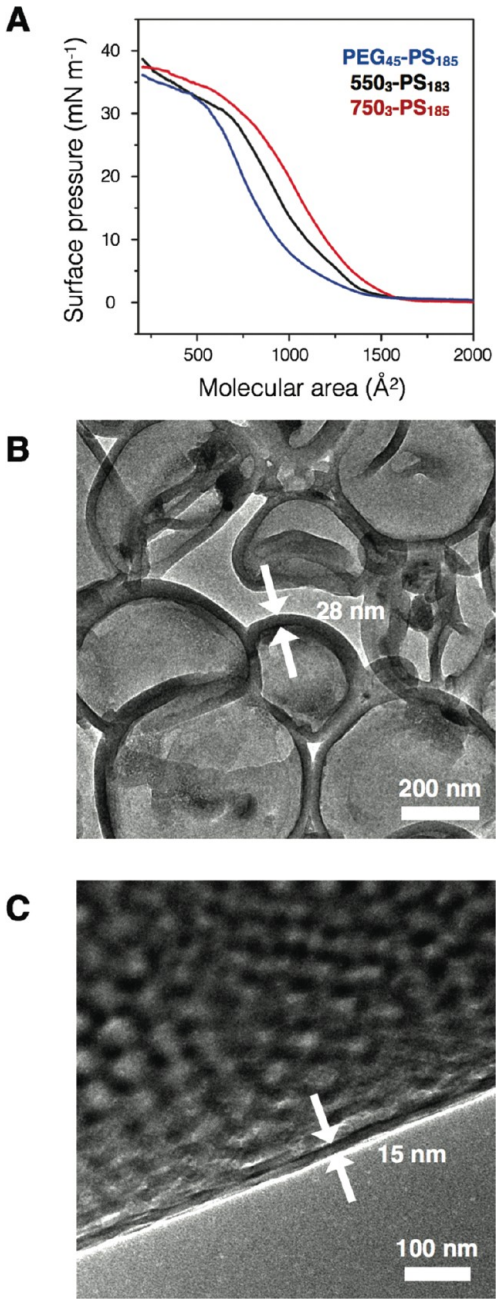

Figure 5. (A) Langmuir isotherms of linear and branched block copolymers. The molecular area was determined by extrapolating the region of increasing surface pressure to the *x*-axis (1080 $Å^2$ for PEG_{45}-PS_{185}, 1340 $Å^2$ for 550_3-PS_{183}, and 1500 $Å^2$ for 750_3-PS_{185}). (B) TEM images of the polymersomes of PEG_{45}-PS_{228} and (C) the polymer cubosomes of 550_3-PS_{212} showing the thickness of the bilayer membrane consisting of the self-assembled structure.

hydrophilic block of bPEG-PS is responsible for the substantially higher area occupied by the BCP in the self-assembled bilayer.

We suspected that the increased molecular area occupied by the branched hydrophilic block in the bilayer could affect the self-assembly behavior of the BCP. TEM images of the polymersomes of PEG_{45}-PS_{228} consistently showed a bilayer membrane with a thickness of ~28 nm (Figure 5B). In comparison, TEM images

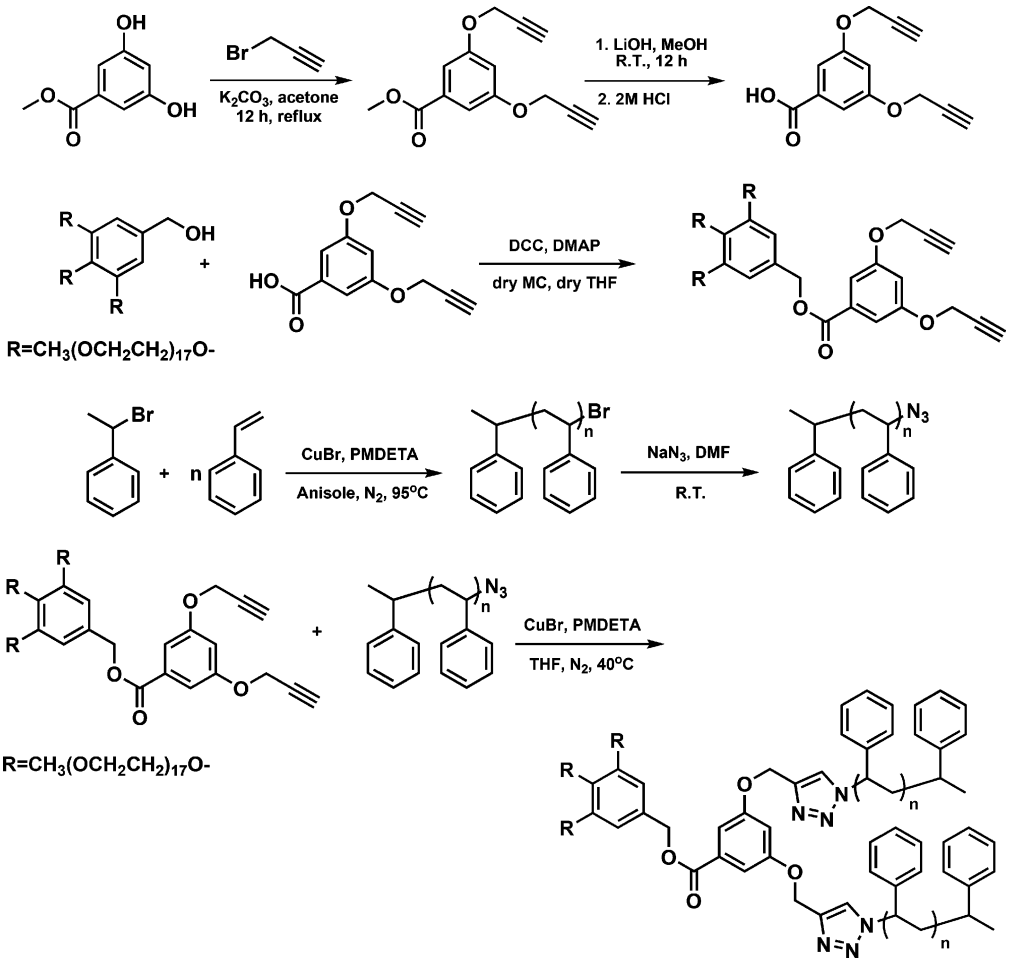

Scheme 2. Synthesis of 750_3-$(PS_n)_2$

of the polymer cubosomes of 550_3-PS_{212} showed that the thickness of the bilayer constituting the inverse cubic mesophases was ~15 nm (Figure 5C). Similarly, we observed that the thickness of the bilayer consisting of the polymer cubosomes of 750_3-PS_{390} was ~24 nm, which was lower than the thickness of the bilayer consisting of the polymersomes of PEG_{45}-PS_{300} (~30 nm) (Figure S7 in the SI). These observations suggest that the increased molecular area of bPEG-PS arising as a result of the branched architecture in the hydrophilic block might force the PS chain to adopt a smaller chain dimension with respect to the plane of the bilayer during self-assembly in the dioxane and water mixture. The smaller chain dimension of the PS chain could reduce the effective length of the hydrophobic block (l_c), which might contribute to an increase in the value of P for the BCP.

Effect of the Length of the Hydrophobic Chain on Self-Assembly. As discussed previously, we suspected that the branched hydrophilic block of bPEG-PS might force the hydrophobic PS chain to adopt a smaller chain dimension during aggregation, as a result of which the BCP would behave as if P exceeds unity. To prove this hypothesis, we synthesized analogues of bPEG-PS containing two PS chains in the hydrophobic block (bPEG-$(PS_n)_2$). By using this architecture, the effective length of the hydrophobic segment is expected to be shortened without a decrease in the molecular weight of the hydrophobic block. We synthesized PS chains containing a terminal azide end group by the ATRP of styrene, followed by the exchange of the bromide end group with NaN_3 in DMF.

^{1}H NMR analysis of PS-N_3 showed a high degree of substitution at the chain end (>90%). The resulting PS-N_3 was used for click chemistry with 750_3-bispropargyl ether (Scheme 2) in the presence of CuBr and *N,N,N′,N″,N″*-pentamethyldiethylenetriamine (PMDETA) in THF. The progress of the click reaction between bispropargyl-750_3 and PS-N_3 was monitored by GPC, which showed complete conversion after 24 h. The resulting 750_3-$(PS_n)_2$ was purified by silica gel chromatography to remove excess PS-N_3 and by preparative GPC. Successful synthesis of 750_3-$(PS_n)_2$ was confirmed by GPC, ^{1}H NMR, and MALDI-TOF mass spectrometry (for details, see the SI).

Upon self-assembly of 750_3-$(PS_{100})_2$ (f_{PEG} = 10.8%) in dioxane (1 wt %) by adding water, we observed the formation of large colloidal particles with an internal

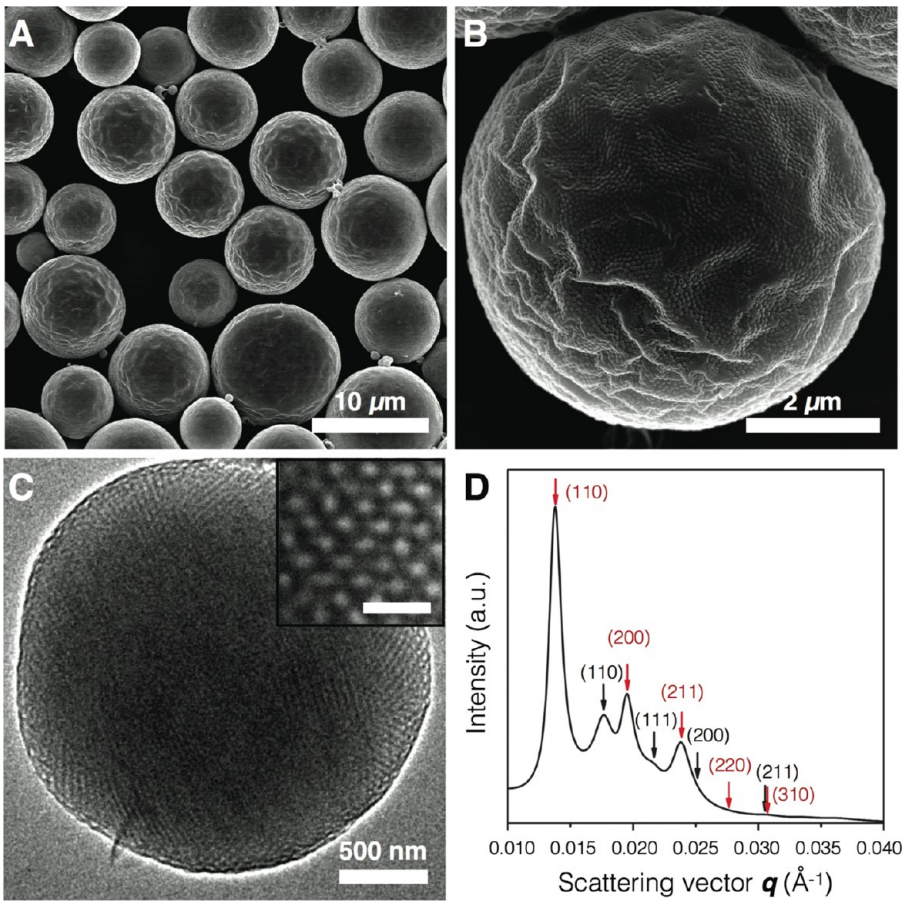

Figure 6. Polymer cubosomes of 750_3-$(PS_{57})_2$. (A and B) SEM images and (C) TEM images of the polymer cubosomes. (D) SAXS results of the polymer cubosomes of 750_3-$(PS_{57})_2$ showing that the internal structures consisted of a mixed phase of *Pn*3*m* (black arrows) and *Im*3*m* (red arrows).

structure consisting of the inverse hexagonal phase (hexasomes). Compared to the formation of hexasomes from the self-assembly of bPEG-PSs such as 550_3-PS_{260} (f_{PEG} = 6.1%) and 750_3-PS_{430} (f_{PEG} = 5.0%), which contained a single PS chain as the hydrophobic block possessing a substantially higher molecular weight, the formation of inverse mesophases of 750_3-$(PS_n)_2$ appeared to be favored over the formation of analogous bPEG-PSs with a single PS chain. This behavior was even more pronounced in the self-assembly of 750_3-$(PS_{57})_2$ (f_{PEG} = 19.7%), where only polymer cubosomes were formed under similar self-assembly conditions (Figure 6A–C). Analysis of the internal crystalline structure of the resulting polymer cubosomes of 750_3-$(PS_{57})_2$ by SAXS showed a mixed phase containing Schwartz P and D surfaces (Figure 6D). Based on the results, we concluded that the branched hydrophilic block played a role in reducing the chain dimension of the PS chain with respect to the plane of the bilayer, which was a result of the increase in the molecular area occupied by bPEG-PS during self-assembly into the BCP bilayer.

Control of the Internal Crystalline Phase by Coassembly. Coassembly of bPEG-PS with a linear PEG-PS containing the desired functional group at the end of the PEG block provides a facile technique for the surface functionalization of polymer cubosomes consisting of self-assembled BCP bilayers.[73,74] When 550_3-PS_{231} and linear PEG_{45}-PS_{210} with an NH_2, SH, or N_3 group at the α-position of the PEG block (Scheme 3) were used for coassembly, the BCP mixture self-assembled into polymer cubosomes with the desired functional group throughout the minimal surface. As shown in Figure 7, the presence of the surface functional group of the polymer cubosomes of 550_3-PS_{231}/PEG_{45}-PS_{210} was confirmed by confocal laser scanning microscopy (CLSM) after reacting the surface functional groups with fluorescence dyes using complementary reactions for the specific functional groups (for details, see the SI).

Interestingly, the average diameter (D_{av}) of the polymer cubosomes of 550_3-PS_{231}/NH_2-PEG_{45}-PS_{210} gradually decreased upon increasing the amount of PEG_{45}-PS_{210} in the BCP mixture. The value of D_{av} of the polymer cubosomes of 550_3-PS_{231}/NH_2-PEG_{45}-PS_{210} decreased from 18.1 μm when 3 wt % of NH_2-PEG_{45}-PS_{210} was used in coassembly to 12.4, 5.8, and 3.8 μm when amounts of NH_2-PEG_{45}-PS_{210} used for coassembly with bPEG-PS were increased to 6, 9, and 12 wt %, respectively (Figure 8A–E). The presence of long PEG chains on the surface of the bilayer would endow

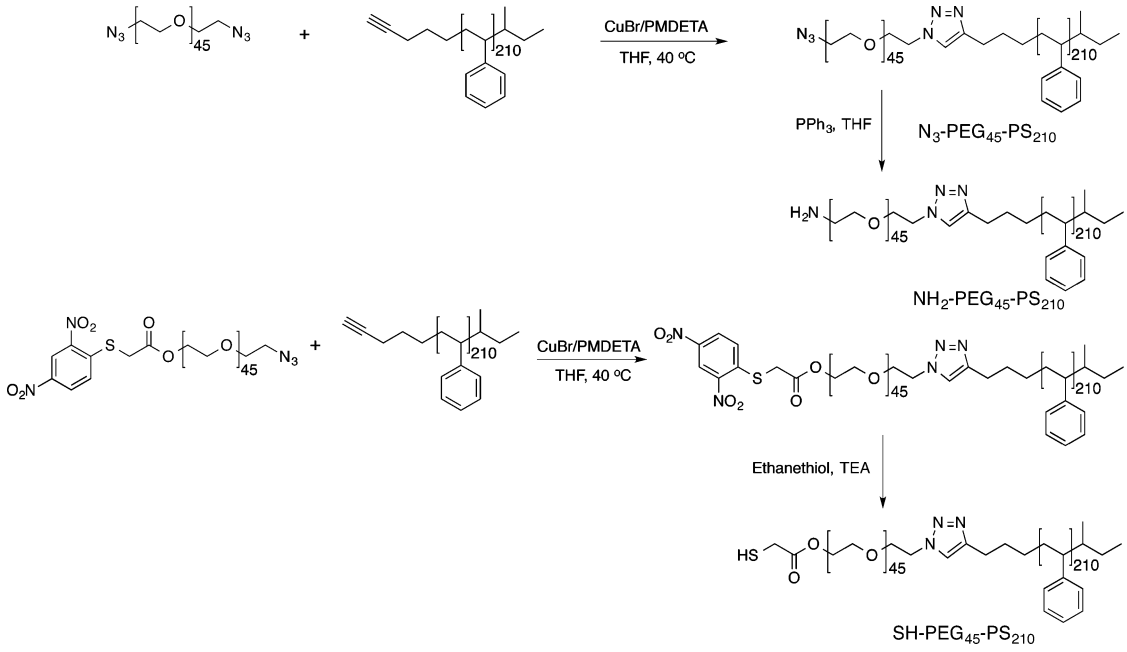

Scheme 3. Synthesis of α-functionalized PEG-PS.

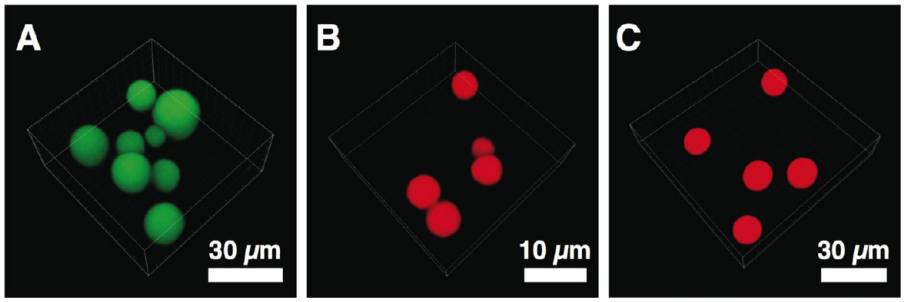

Figure 7. CLSM images of surface-functionalized polymer cubosomes prepared by the coassembly of 550_3-PS_{231} and (A) NH_2-PEG_{45}-PS_{210} (7 wt %, labeled with NHS-fluorescein), (B) SH-PEG_{45}-PS_{210} (10 wt %, labeled with rhodamine-maleimide), and (C) N_3-PEG_{45}-PS_{210} (9 wt %, labeled with rhodamine-alkyne).

colloidal stability of the polymer cubosomes, which would lead to a decrease in the diameter of the polymer cubosomes.[39,40] When we examined the internal crystalline structure of the resulting polymer cubosomes, we found that the internal structure of the inverse bicontinuous cubic phase transformed from a Schwartz D surface (*Pn*3*m*, a = 49.0 nm) to a Schwartz P surface (*Im*3*m*, a = 94.6 nm), as the amount of NH_2-PEG_{45}-PS_{210} increased from 3 wt % to 12 wt % (Figure 8F). This transition in the internal crystalline structure of inverse mesophases was in accordance with the phase transition of the inverse mesophases of lipids upon the decrease in the local curvature of the lipid bilayer. Therefore, we inferred that the addition of a linear BCP reduces the effective molecular area (a_0) of the BCP mixture, which might contribute to a change in the structure of the mesophase exhibiting more local negative curvature (*Pn*3*m*), relative to the structure attributed to the mesophase with a lower curvature (*Im*3*m*). This result also agrees with the transition of the internal structure from the Schwartz D surface (*Pn*3*m*) of the polymer cubosomes of 550_3-PS_{231} to a Schwartz P surface (*Im*3*m*) found in the polymer cubosomes of 550_3-PS_{212}.

CONCLUSIONS

The solution self-assembly of BCPs into well-defined inverse cubic mesophases is an emerging method for the direct synthesis of highly porous polymers with triply periodic mesoporous networks. We synthesized branched−linear BCPs containing a simple branched hydrophilic block with three PEG chains as the hydrophile (bPEG-PS). These BCPs were utilized as model systems to examine the effect of the architecture of the BCPs on their self-assembly behavior. The branched architecture in the hydrophilic block was responsible for the preferential self-assembly of the BCPs into inverse cubic mesophases. The block ratio (f_{PEG}) was the primary structural factor determining the phase behavior of the BCP. The branched architecture of the hydrophilic block allowed the design of BCPs favoring self-assembly into inverse mesophases, without deviating from the optimal value of f_{PEG} required for

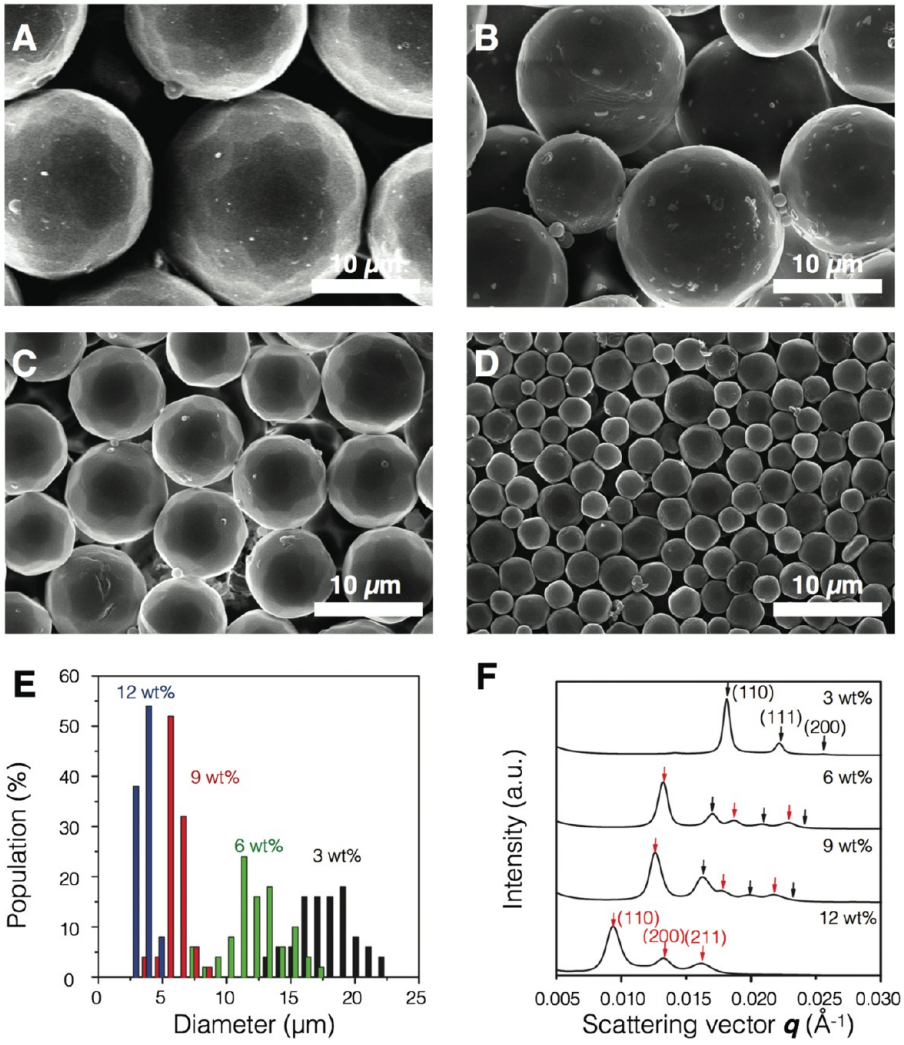

Figure 8. Structural transformation of the polymersomes prepared by the coassembly of 550_3-PS_{231} and varying amounts of NH_2-PEG_{45}-PS_{210}. (A–D) SEM images of the polymersomes of 550_3-PS_{231}/NH_2-PEG_{45}-PS_{210} showing a decrease in the average diameter with an increase in the amount of NH_2-PEG_{45}-PS_{210} used for coassembly (A, 97:3 w/w; B, 94:6 w/w; C, 91:9 w/w; and D, 88:12 w/w). (E) Distribution of the diameter of the polymer cubosomes of 550_3-PS_{231}/NH_2-PEG_{45}-PS_{210}. The values of D_{av} were 18.1 μm (3 wt % NH_2-PEG_{45}-PS_{210}), 12.4 μm (6 wt %), 5.8 μm (9 wt %), and 3.8 μm (12 wt %). (E) SAXS results of the polymer cubosomes of 550_3-PS_{231}/NH_2-PEG_{45}-PS_{210} showing the transition of the internal crystalline structure from a D surface (*Pn*3*m*, $a = 49.0$ nm) to a P surface (*Im*3*m*, $a = 94.6$ nm), depending on the amount of linear BCP used for coassembly. The red and black arrows indicate *Im*3*m* and *Pn*3*m* symmetry, respectively.

self-assembly. For hydrophilic PEG domains with a fixed molecular weight, the increase in the molecular weight of the hydrophobic PS chain caused a transition of the self-assembled structures, from flat lamellar and polymer vesicles to inverse mesophases (P surface and D surface) and inverse hexagonal phase (H_{II}). This structural transformation of self-assembled structures was reminiscent of the morphological transition of micelles and vesicles in the solution self-assembly of conventional BCPs. The coassembly of bPEG-PS and their linear analogues allowed a facile surface functionalization of inverse cubic mesophases as well as control of the internal crystalline structure of polymer cubosomes, by altering local curvature of the BCP bilayers consisting of the inverse cubic mesophase. The results described here may provide a means for designing BCPs with diverse chemical structures in order to preferentially form inverse bicontinuous cubic crystalline structures in solution. This could be a new technique for creating porous polymers with well-defined reticulated pore structures and surface functionality.

MATERIALS AND METHODS

General Methods. Unless otherwise noted, all reagents and chemicals were used as received from Sigma-Aldrich and TCI. DMF was dried over CaH_2 under N_2 and freshly distilled prior to use. Tetrahydrofuran (THF) was refluxed over a mixture of Na and benzophenone under N_2 and distilled before use. All reactions were performed under N_2 unless otherwise noted. ^1H and ^{13}C NMR spectra were recorded on a Varian VNMRS 600

spectrometer, using CD_2Cl_2 and $CDCl_3$ as solvents. Matrix-assisted laser desorption ionization time-of-flight mass spectroscopy (MALDI-TOF-MS) was performed on a Bruker Ultraflex III TOF-TOF mass spectrometer equipped with a nitrogen laser (335 nm). Scanning electron microscopy (SEM) was performed on a FEI Nova NanoSEM 230 microscope and Hitachi S-4800 FE SEM at an acceleration voltage of 10 kV. The dried polymer cubosomes were placed on a conductive carbon tape and then coated with Pt with a thickness of 3 nm by using a K575X sputter coater. Transmission electron microscopy was recorded on a JEOL JEM-2100 microscope at 200 kV. Specimens were prepared by placing a drop of the polymer cubosome solution on a carbon-coated Cu grid (200 mesh, EM Science). After 30 min, the remaining solution on the grid was removed with a filter paper, and the grid was air-dried overnight. Confocal laser scanning fluorescence microscopy was performed on a FluoView 1000 confocal microscope (Olympus). Synchrotron SAXS and Image Synchrotron small-angle X-ray scattering data were obtained on PLS-II 9A at Pohang Acceleration Laboratory (Pohang, Korea). The particle size distribution of polymer cubosomes was measured by analyzing SEM images of polymer cubosomes with ImageJ software. One hundred particles were selected for the image analysis from SEM images taken from 5−10 different positions.

Langmuir Isotherms and Porosimetry. The Langmuir isotherms were obtained using a film balance (KSV NIMA) with a platinum Wilhelmy plate. The subphase was maintained at 20 (±0.5) °C. Typically, the polymer solution (40 μL, 1 mg mL^{-1}) was spread evenly over the water surface in small drops. After a 5 min delay to allow for the solvent evaporation, compression was applied at a constant rate of 10 mm min^{-1} (12.5 mm^2 s^{-1}). Surface analysis of the mesoporous cubosomes was performed by nitrogen sorption isotherms at −196 °C using a BEL BELSORP-Max system. The surface area and pore size distributions were estimated by using the BET equation and the BJH method, respectively.

Synthesis of Macroinitiators and Block Copolymers. Synthetic procedures and characterization data for all compounds and block copolymers were provided in detail in the SI.

Cosolvent Method for Self-Assembly of bPEG-PSs. A typical procedure is provided: The bPEG-PS was initially dissolved in 2 mL of 1,4-dioxane (1 wt %) in a capped vial, and the solution was stirred for 3 h at room temperature. Water (total 2 mL) was added at a controlled rate (1 mL h^{-1}) to the solution *via* a syringe pump with vigorous stirring (850 rpm). The resulting milky suspension was dialyzed (molecular weight cutoff (MWCO) = 12−14 kDa, SpectraPor) against water for 24 h to remove the organic solvent. For coassembly of bPEG-PS and α-functional PEG-PS, a dioxane solution of the mixture of two block copolymers was prepared by mixing two stock solutions (concentration of 10 mg mL^{-1}) of the block copolymers. The resulting solution of a mixture of block copolymers was allowed to equilibrate for 12 h at room temperature.

Dye Labeling of Surface Functional Groups of Polymer Cubosomes. Polymer cubosomes (10 mg mL^{-1}, 550_3-PS_{231}/SH-PEG_{45}-PS_{210} or 550_3-PS_{231}/NH_2-PEG_{45}-PS_{210}) in PBS (pH 7.4) were mixed with dye solution (F-MI or Rho-NHS in PBS, 200 equiv to SH or NH_2 groups). The mixtures were aged at room temperature for 1 day and then transferred into the centrifugal tubes with a centrifugal filter (MWCO = 100 kDa, Amicon). After repeated centrifugation, the excess dyes were removed from the suspension. 550_3-PS_{231}/N_3-PEG_{45}-PS_{210} (10 mg mL^{-1} in PBS) was aged with Rho-alkyne (50 equiv to azide groups) in the presence of $CuSO_4 \cdot 5H_2O$ (3 equiv to alkyne groups) and L-ascorbic sodium salt (10 equiv to alkyne groups) for 1 day under a nitrogen atmosphere. The solution was purified by repeated centrifugation, as described above.

Conflict of Interest: The authors declare no competing financial interest.

Supporting Information Available: Synthetic procedures, characterization data of compounds and block copolymers, and additional electron microscopy images. This material is available free of charge *via* the Internet at http://pubs.acs.org.

Acknowledgment. This research was supported by National Research Foundation (NRF) of Korea (NRF-2013R1A1A013075) and UNIST (UMI Future Challenge Grant). C.P. acknowledges NRF for the research fellowship (2013R1A1A2063049). K.T.K. also thanks KUCC for financial support (2 V03280). We thank UCRF and UOBC for microscopy facilities.

REFERENCES AND NOTES

1. Hamley, I. W. *Block Copolymers in Solution: Fundamentals and Applications*; Wiley: Chichester, 2005.
2. Schacher, F. H.; Rupar, P. A.; Manners, I. Functional Block Copolymers: Nanostructured Materials with Emerging Applications. *Angew. Chem., Int. Ed.* **2012**, *51*, 7898–7921.
3. Rösler, A.; Vandermeulen, G. W. M.; Klok, H.-A. Advanced Drug Delivery Devices via Self-Assembly of Amphiphilic Block Copolymers. *Adv. Drug Delivery Rev.* **2001**, *53*, 95–108.
4. Holder, S. J.; Sommerdijk, N. A. J. M. New Micellar Morphologies from Amphiphilic Block Copolymers: Disks, Toroids, and Bicontinuous Micelles. *Polym. Chem.* **2011**, *2*, 1018–1028.
5. Elsabahy, M.; Wooley, K. L. Design of Polymeric Nanoparticles for Biomedical Delivery Applications. *Chem. Soc. Rev.* **2012**, *41*, 2545–2561.
6. Mai, Y.; Eisenberg, A. Self-Assembly of Block Copolymers. *Chem. Soc. Rev.* **2012**, *41*, 5969–5985.
7. Zhang, L.; Eisenberg, A. Multiple Morphologies of "Crew-Cut" Aggregates of Amphiphilic Block Copolymers. *Science* **1995**, *268*, 1728–1731.
8. van Hest, J. C. M.; Delnoye, D. A. P.; Baars, M. W. P. L.; van Genderen, M. H. P.; Meijer, E. W. Polystyrene-Dendrimer Amphiphilic Block Copolymers with a Generation-Dependent Aggregation. *Science* **1995**, *268*, 1592–1595.
9. Israelachvili, J. N. *Intermolecular and Surface Forces*, 3rd ed.; Academic Press: Amsterdam, 1992.
10. Israelachvili, J. N.; Mitchell, D. J.; Ninham, B. W. Theory of Self-Assembly of Hydrocarbon Amphiphiles into Micelles and Bilayers. *J. Chem. Soc., Faraday Trans. 2* **1976**, *72*, 1525–1568.
11. Zhu, J.; Zhang, S.; Zhang, K.; Wang, X.; Mays, J. W.; Wooley, K. L.; Pochan, D. J. Disk-cylinder and Disk-sphere Nanoparticles via a Block Copolymer Blend Solution Construction. *Nat. Commun.* **2013**, *4*, 2297.
12. Pochan, D. J.; Chen, Z.; Cui, H.; Hales, K.; Qi, K.; Wooley, K. L. Toroidal Triblock Copolymer Assembly. *Science* **2004**, *306*, 94–97.
13. Won, Y.-Y.; Davis, H. T.; Bates, F. S. Giant Wormlike Rubber Micelles. *Science* **1999**, *283*, 960–963.
14. Discher, B. M.; Won, Y.-Y.; Ege, D. S.; Lee, J. C-M.; Bates, F. S.; Discher, D. E.; Hammer, D. A. Polymersomes: Tough Vesicles Made from Diblock Copolymers. *Science* **1999**, *284*, 1143–1146.
15. Jain, S.; Bates, F. S. On the Origin of Morphological Complexity in Block Copolymer Surfactants. *Science* **2003**, *300*, 460–464.
16. Cui, H.; Chen, Z.; Zhong, S.; Wooley, K. L.; Pochan, D. J. Block Copolymer Assembly via Kinetic Control. *Science* **2007**, *317*, 647–650.
17. Hales, K.; Chen, Z.; Wooley, K. L.; Pochan, D. J. Nanoparticles with Tunable Internal Structure from Triblock Copolymers of PAA-b-PMA-b-PS. *Nano Lett.* **2008**, *8*, 2023–2026.
18. Li, Z.; Kesselman, E.; Talmon, Y.; Hillmyer, M. A.; Lodge, T. P. Multicompartment Micelles from ABC Miktoarm Stars in Water. *Science* **2004**, *306*, 98–101.
19. Christian, D. A.; Tian, A.; Ellenbroek, W. G.; Levental, I.; Rajagopal, K.; Janmey, P. A.; Liu, A. J.; Baumgart, T.; Discher, D. E. Spotted Vesicles, Striped Micelles and Janus Assemblies Induced by Ligand Binding. *Nat. Mater.* **2009**, *8*, 843–849.
20. Wang, X.; Guerin, G.; Wang, H.; Wang, Y.; Manners, I.; Winnik, M. A. Cylindrical Block Copolymer Micelles and Co-micelles of Controlled Length and Architecture. *Science* **2007**, *317*, 644–647.
21. Jia, L.; Zhao, G.; Shi, W.; Coombs, N.; Gourevich, I.; Walker, G. C.; Guerin, G.; Manners, I.; Winnik, M. A Design Strategy for the Hierarchical Fabrication of Colloidal Hybrid Mesostructures. *Nat. Commun.* **2014**, *5*, 3882.

22. Hudson, Z. M.; Lunn, D. J.; Winnik, M. A.; Manners, I. Colour-Tunable Fluorescent Multiblock Micelles. *Nat. Commun.* **2014**, *5*, 3372.
23. Rupar, P. A.; Chabanne, L.; Winnik, M. A.; Manners, I. Non-Centrosymmetric Cylindrical Micelles by Unidirectional Growth. *Science* **2012**, *337*, 559–562.
24. Kim, H.; Kang, Y. J.; Kang, S.; Kim, K. T. Monosaccharide-Responsive Release of Insulin from Polymersomes of Polyboroxole Block Copolymers at Neutral pH. *J. Am. Chem. Soc.* **2012**, *134*, 4030–4033.
25. Battaglia, G.; Ryan, A. J. Effect of Amphiphile Size on the Transformation from a Lyotropic Gel to a Vesicular Dispersion. *Macromolecules* **2006**, *39*, 798–805.
26. Battaglia, G.; Ryan, A. J. The Evolution of Vesicles from Bulk Lamellar Gels. *Nat. Mater.* **2005**, *4*, 869–876.
27. Alexandridis, P.; Olsson, U.; Lindman, B. Structural Polymorphism of Amphiphilic Copolymers: Six Lyotropic Liquid Crystalline and Two Solution Phases in a Poly(oxybutylene)-b-poly(oxyethylene)−Water−Xylene System. *Langmuir* **1997**, *13*, 23–34.
28. Jain, S.; Gong, X.; Scriven, L. E.; Bates, F. S. Disordered Network State in Hydrated Block-Copolymer Surfactants. *Phys. Rev. Lett.* **2006**, *96*, 138304.
29. Larsson, K. Cubic Lipid-Water Phases: Structures and Biomembrane Aspects. *J. Phys. Chem.* **1989**, *93*, 7304–7314.
30. Kulkarni, C. V.; Wachter, W.; Iglesias-Salto, G.; Engelskirchen, S.; Ahualli, S. Monoolein: a Magic Lipid? *Phys. Chem. Chem. Phys.* **2011**, *13*, 3004–3021.
31. Seddon, J. M.; Robins, J.; Gulik-Krzywicki, T.; Delacroix, H. Inverse Micellar Phases of Phospholipids and Glycolipids. *Phys. Chem. Chem. Phys.* **2000**, *2*, 4485–4493.
32. Scriven, L. E. Equilibrium Bicontinuous Structure. *Nature* **1976**, *263*, 123–125.
33. Larsson, K. Two Cubic Phases in Monoolein-Water System. *Nature* **1983**, *304*, 664.
34. Mackay, A. L. Periodic Minimal Surfaces. *Physica* **1985**, *131B*, 300–305.
35. Larsson, K.; Tiberg, F. Periodic Minimal Surface Structures in Bicontinuous Lipid-Water Phases and Nanoparticles. *Curr. Opin. Colloid Interface Sci.* **2005**, *9*, 365–369.
36. Almsherqi, Z. A.; Kohlwein, S. D.; Deng, Y. Cubic Membranes: A Legend beyond the Flatland of Cell Membrane Organization. *J. Cell Biol.* **2006**, *173*, 839–844.
37. Deng, Y.; Mieczkowski, M. Three-Dimensional Periodic Cubic Membrane Structure in the Mitochondria of Amoebae-Chaos Carolinensis. *Protoplasma* **1998**, *203*, 16–25.
38. Gustavsson, J.; Ljusberg-Wahren, H.; Almgren, M.; Larsson, K. Cubic Lipid-Water Phase Dispersed into Submicron Particles. *Langmuir* **1996**, *12*, 4611–4613.
39. Gustavsson, J.; Ljusberg-Wahren, H.; Almgren, M.; Larsson, K. Submicron Particles of Reversed Lipid Phases in Water Stabilized by a Nonionic Amphiphilic Polymer. *Langmuir* **1997**, *13*, 6964–6971.
40. Barauskas, J.; Johnsson, M.; Joabsson, F.; Tiberg, F. Cubic Phase Nanoparticles (Cubosome): Principles for Controlling Size, Structure, and Stability. *Langmuir* **2005**, *21*, 2569–2577.
41. Spicer, P. T. Progress in Liquid Crystalline Dispersions: Cubosomes. *Curr. Opin. Colloid Interface Sci.* **2005**, *10*, 274–279.
42. Landau, E. M.; Rosenbusch, J. P. Lipidic Cubic Phases: A Novel Concept for the Crystallization of Membrane Proteins. *Proc. Natl. Acad. Sci. U.S.A.* **1996**, *93*, 14532–14535.
43. Caffrey, M. Crystallizing Membrane Proteins for Structure Determination: Use of Lipidic Mesophases. *Annu. Rev. Biophys.* **2009**, *38*, 29–51.
44. Mezzenga, R.; Schurtenberger, P.; Burbridge, A.; Michel, M. Understanding Foods as Soft Materials. *Nat. Mater.* **2005**, *4*, 729–740.
45. Fong, W. K.; Salentinig, S.; Prestidge, C. A.; Mezzenga, R.; Hawley, A.; Boyd, B. J. Generation of Geometrically Ordered Lipid-Based Liquid-Crystalline Nanoparticles Using Biologically Relevant Enzymatic Processing. *Langmuir* **2014**, *30*, 5373–5377.
46. Salentinig, S.; Phan, S.; Khan, J.; Hawley, A.; Boyd, B. J. Formation of Highly Organized Nanostructures during the Digestion of Milk. *ACS Nano* **2013**, *7*, 10904–10911.
47. Salentinig, S.; Phan, S.; Hawley, A.; Boyd, B. J. Self-Assembly Structure Formation during the Digestion of Human Breast Milk. *Angew. Chem., Int. Ed.* **2015**, *54*, 1600–1603.
48. Angelova, A.; Angelov, B.; Papahadjopoulos-Sternberg, B.; Ollivon, M.; Bourgaux, C. Proteocubosomes: Nanoporous Vehicles with Tertiary Organized Fluid Interfaces. *Langmuir* **2005**, *21*, 4138–4143.
49. Angelov, B.; Angelova, A.; Papahadjopoulos-Sternberg, B.; Lesieur, S.; Sadoc, J.-F.; Ollivon, M.; Couvreur, P. Detailed Structure of Diamond-Type Lipid Cubic Nanoparticles. *J. Am. Chem. Soc.* **2006**, *128*, 5813–5817.
50. Angelova, A.; Angelov, B.; Mutafchieva, R.; Sesieur, S.; Couvreur, P. Self-Assembled Multicompartment Liquid Crystalline Lipid Carriers for Protein, Peptide, and Nucleic Acid Drug Delivery. *Acc. Chem. Res.* **2011**, *44*, 147–156.
51. Clogston, J.; Caffrey, M. Controlling Release from the Lipidic Cubic Phase. Amino Acids, Peptides, Proteins and Nucleic Acids. *J. Controlled Release* **2005**, *107*, 97–111.
52. Guo, C.; Wnag, J.; Cao, F.; Lee, R. J.; Zhai, G. Lyotropic Liquid Crystal Systems in Drug Delivery. *Drug Discovery Today* **2010**, *15*, 1032–1040.
53. Chung, H.; Kim, J.; Um, J. Y.; Kwon, I. C.; Jeong, S. Y. Self-Assembled "Nanocubicle" as a Peroral Insulin Delivery. *Diabetologia* **2002**, *45*, 448–451.
54. Negrini, R.; Mezzenga, R. pH-Responsive Lyotropic Liquid Crystals for Controlled Drug Delivery. *Langmuir* **2011**, *27*, 5296–5303.
55. Deshpande, S.; Venugopal, E.; Ramagiri, S.; Bellare, J. R.; Kumaraswamy, G.; Singh, N. Enhancing Cubosome Functionality by Coating with a Single Layer of Poly-ε-lysine. *ACS Appl. Mater. Interfaces* **2014**, *6*, 17126–17133.
56. Gong, X.; Moghaddam, M. J.; Sagnella, S. M.; Conn, C. E.; Danon, S. J.; Waddington, L. J.; Drummond, C. J. Lyotropic Liquid Crystalline Self-Assembly Material Behavior and Nanoparticulate Dispersions of a Phytanyl Pro-Drug Analogue of Capecitabine−A Chemotherapy Agent. *ACS Appl. Mater. Interfaces* **2011**, *3*, 1552–1561.
57. Nazaruk, E.; Szlęzak, M.; Górecka, E.; Bilewicz, R.; Osornia, Y. M.; Uebelhart, P.; Landau, E. M. Design and Assembly of pH-Sensitive Lipidic Cubic Phase Matrices for Drug Release. *Langmuir* **2014**, *30*, 1383–1390.
58. Duhem, N.; Danhier, F.; Pourcelle, V.; Schumers, J.-M.; Bertrand, O.; LeDuff, C. S.; Hoeppener, S.; Schubert, U. S.; Gohy, J.-F.; Marchand-Brynaert, J.; *et al*. Self-Assembling Doxorubicin-Tocopherol Succinate Prodrug as a New Drug Delivery System: Synthesis, Characterization, and in Vitro and in Vivo Anticancer Activity. *Bioconjugate Chem.* **2014**, *25*, 72–81.
59. Svensson, O.; Thuresson, K.; Arnebrant, T. Interactions between Drug Delivery Particles and Nucin in Solution and at Interfaces. *Langmuir* **2008**, *24*, 2573–2579.
60. Zhen, G.; Hinton, T. M.; Muir, B. W.; Shi, S.; Tizard, M.; McLean, K. M.; Hartley, P. G.; Gunatillake, P. Glycerol Monooleate-Based Nanocarriers for siRNA Delivery in Vitro. *Mol. Pharmaceutics* **2012**, *9*, 2450–2457.
61. Caltagirone, C.; Falchi, A. M.; Lampis, S.; Lippolis, V.; Meli, V.; Monduzzi, M.; Prodi, L.; Schmidt, J.; Sgarzi, M.; Talmon, Y.; Bizzarri, R.; Murgia, S. Cancer-Cell-Targeted Theranostic Cubosomes. *Langmuir* **2014**, *30*, 6228–6236.
62. Dehsorkhi, A.; Castelletto, V.; Hamley, I. W.; Harris, P. J. F. Multiple Hydrogen Bonds Induce Formation of Nanoparticles with Internal Microemulsion Structure by an Amphiphilic Copolymer. *Soft Matter* **2011**, *7*, 10116–10121.
63. Zhang, L.; Bartels, C.; Yu, Y.; Shen, H.; Eisenberg, A. Mesosized Crystal-like Structure of Hexagonally Packed Hollow Hoops by Solution Self-Assembly of Diblock Copolymers. *Phys. Rev. Lett.* **1997**, *79*, 5034–5037.
64. Yu, K.; Bartels, C.; Eisenberg, A. Trapping of Intermediate Structures of the Morphological Transition of Vesicles to Inverted Hexagonally Packed Rods in Dilute Solutions of PS-b-PEO. *Langmuir* **1999**, *15*, 7157–7167.

65. Yu, K.; Bartels, C.; Eisenberg, A. Vesicles with Hollow Rods in the Walls: A Trapped Intermediate Morphology in the Transition of Vesicles to Inverted Hexagonally Packed Rods in Dilute Solutions of PS-b-PEO. *Macromolecules* **1998**, *31*, 9399–9402.
66. McKenzie, B. E.; Nudelman, F.; Bomans, P. H. H.; Holder, S. J.; Sommerdijk, N. A. J. M. Temperature-Responsive Nanospheres with Bicontinuous Internal Structures from a Semicrystalline Amphiphilic Block Copolymer. *J. Am. Chem. Soc.* **2010**, *132*, 10256–10259.
67. McKenzie, B. E.; de Visser, J. F.; Friedrich, H.; Wirix, M. J. M.; Bomans, P. H. H.; de With, G.; Holder, S. J.; Sommerdijk, N. A. J. M. Bicontinuous Nanospheres from Simple Amorphous Amphiphilic Diblock Copolymers. *Macromolecules* **2013**, *46*, 9845–9848.
68. McKenzie, B. E.; Friedrich, H.; Wirix, M. J. M.; de Visser, J.; Monaghan, O. R.; Bomans, P. H. H.; Nudelman, F.; Holder, S. J.; Sommerdijk, N. A. J. M. Controlling Internal Pore Sizes in Bicontinuous Polymeric Nanospheres. *Angew. Chem., Int. Ed.* **2015**, *54*, 2457–2461.
69. Holder, S. J.; Woodward, G.; McKenziea, B.; Sommerdijk, N. A. J. M. Semi-crysatlline Block Copolymer Bicontinuous Nanospheres for Thermoresponsive Controlled Release. *RSC Adv.* **2014**, *4*, 26354–26358.
70. McKenzie, B. E.; Holder, S. J.; Sommerdijk, N. A. J. M. Assessing Internal Structure of Polymer Assemblies from 2D to 3D CryoTEM: Bicontinuous Micelles. *Curr. Opin. Colloid Interface Sci.* **2012**, *17*, 343–349.
71. Denkova, A. G.; Bomans, P. H. H.; Coppens, M.-O.; Sommerdijk, N. A. J. M.; Mendes, E. Complex Morphologies of Self-Assembled Block Copolymer Micelles in Binary Solvent Mixtures: The Role of Solvent-Solvent Correlations. *Soft Matter* **2011**, *7*, 6622–6628.
72. Parry, A. L.; Bomans, P. H. H.; Holder, S. J.; Sommerdijk, N. A. J. M.; Biagini, S. C. G. Cryo Electron Tomography Reveals Confined Complex Morphologies of Tripeptide-Containing Amphiphilic Double-Comb Diblock Copolymers. *Angew. Chem., Int. Ed.* **2008**, *47*, 8859–8862.
73. La, Y.; Park, C.; Shin, T. J.; Joo, S. H.; Kang, S.; Kim, K. T. Colloidal Inverse Bicontinuous Cubic Membranes of Block Copolymers with Tunable Surface Functional Groups. *Nat. Chem.* **2014**, *6*, 534–541.
74. Park, C.; La, Y.; An, T. H.; Jeong, H. Y.; Kang, S.; Joo, S. H.; Ahn, H.; Shin, T. J.; Kim, K. T. Mesoporous Monoliths of Inverse Bicontinuous Cubic Phases of Block Copolymer Bilayers. *Nat. Commun.* **2015**, *6*, 6392.
75. Schoen, A. H. *Technical Report No. TN D-5541*; NASA: Washington, D.C., **1970**.
76. Yu, H.; Qiu, X.; Nunes, S. P.; Peinemann, K.-V. Biomimetic Block Copolymer Particles with Gated Nanopores and Ultrahigh Protein Sorption Capacity. *Nat. Commun.* **2014**, *5*, 4110.
77. Cai, H.; Jiang, G.; Shen, Z.; Fan, X. Solvent-Induced Hierarchical Self-Assembly of Amphiphilic PEG(G_m)-b-PS Dendritic-Linear Block Copolymers. *Soft Matter* **2013**, *9*, 11398–11404.
78. Cai, H.; Jiang, G.; Chen, C.; Li, Z.; Shen, Z.; Fan, X. New Morphologies and Phase Transitions of Rod-Coil Dendritic-Linear Block Copolymers Depending on Dendron Generation and Preparation Procedure. *Macromolecules* **2014**, *47*, 146–151.
79. Percec, V.; Wilson, D. A.; Leowanawat, P.; Wilson, C. J.; Hughes, A. D.; Kaucher, M. S.; Hammer, D. A.; Levine, D. H.; Kim, A. J.; Bates, F. S.; *et al*. Self-Assembly of Janus Dendrimers into Uniform Dendrimersomes and Other Complex Architectures. *Science* **2010**, *328*, 1009–1014.
80. Peterca, M.; Percec, V.; Leowanawat, P.; Bertin, A. Predicting the Size and Properties of Dendrimersomes from the Lamellar Structure of Their Amphiphilic Janus Dendrimers. *J. Am. Chem. Soc.* **2011**, *133*, 20507–20520.
81. Percec, V.; Leowanawat, P.; Sun, H.-J.; Kulikov, O.; Nusbaum, C. D.; Tran, T. M.; Bertin, A.; Wilson, D. A.; Peterca, M.; Zhang, S.; *et al*. Modular Synthesis of Amphiphilic Janus Glycodendrimers and Their Self-Assembly into Glycodendrimersomes and Other Complex Architectures with Bioactivity to Biomedically Relevant Lectins. *J. Am. Chem. Soc.* **2013**, *135*, 9055–9077.
82. Zhang, S.; Sun, H.-J.; Hughes, A. D.; Draghici, B.; Lejnieks, J.; Leowanawat, P.; Bertin, A.; De Leon, L. O.; Kulikov, O. V.; Chen, Y.; *et al*. "Single-Single" Amphiphilic Janus Dendrimers Self-Assemble into Uniform Dendrimersomes with Predictable Size. *ACS Nano* **2014**, *8*, 1554–1565.
83. Jeong, M. G.; van Hest, J. C. M.; Kim, K. T. Self-Assembly of Dendritic-Linear Block Copolymers with Fixed Molecular Weight and Block Ratio. *Chem. Commun.* **2012**, *48*, 3590–3592.
84. Lutz, J.-F.; Akdemir, Ö; Hoth, A. Point by Point Comparison of Two Thermosensitive Polymers Exhibiting a Similar LCST: Is the Age of Poly(NIPAM) Over? *J. Am. Chem. Soc.* **2006**, *128*, 13046–13047.
85. Lutz, J.-F. Polymerization of Oligo(ethynele glycol) (meth)acrylates: Toward New Generations of Smart Biocompatible Materials. *J. Polym. Sci., Part A: Polym. Chem.* **2008**, *46*, 3459–3470.
86. Kulkarni, C. V.; Tang, T.-Y.; Seddon, A. M.; Seddon, J. M.; Cesa, O.; Templer, R. H. Engineering Bicontinuous Cubic Structures at the Nanoscale—the Role of Chain Splay. *Soft Matter* **2010**, *6*, 3191–3194.
87. Manni, L. S.; Zabara, A.; Osornio, Y. M.; Schöppe, J.; Batyuk, A.; Plückthun, A.; Siegel, J. S.; Mezzenga, R.; Landau, E. M. Phase Behavior of a Designed Cyclopropyl Analogue of Monoolein: Implications for Low-Temperature Membrane Protein Crystallization. *Angew. Chem., Int. Ed.* **2015**, *54*, 1027–1031.
88. Cox, J. K.; Yu, K.; Constantine, B.; Eisenberg, A.; Lennox, R. B. Polystyrene—Poly(ethylene oxide) Diblock Copolymers Form Well-Defined Surface Aggregates at the Air/Water Interface. *Langmuir* **1999**, *15*, 7714–7718.